RSC Advances

PAPER

View Article Online
View Journal | View Issue

Cite this: *RSC Adv.*, 2018, **8**, 1210

A facile synthesis of a cobalt nanoparticle–graphene nanocomposite with high-performance and triple-band electromagnetic wave absorption properties

Qin Long, Zhiqiang Xu, Huanhuan Xiao and Kenan Xie *

Ferromagnetic metal nanoparticle/graphene nanocomposites are promising as excellent electromagnetic (EM) wave absorption materials. In this work, we used a facile method to synthesize a cobalt nanoparticle–graphene (CoNP–G) nanocomposite. The obtained CoNPs–G exhibited a saturation magnetization (M_s) of 31.3 emu g^{-1} and a coercivity (H_C) of 408.9 Oe at 298.15 K. In particular, the CoNPs–G nanocomposite provided high-performance EM wave absorption with multiband, wide effective absorption bandwidth, which was mainly attributed to the synergy effects generated by the magnetic loss of cobalt and the dielectric loss of graphene. In the range of 2–18 GHz, the sample (55 wt% CoNPs–G) held three effective reflection loss (RL) peaks (frequency ranges of 2.4–3.84, 7.84–11.87 and 13.25–18 GHz, respectively, RL ≤ −10 dB) with the coating thickness of 4.5 mm, and the effective bandwidth reached the maximum of 10.22 GHz, and the minimal RL reached −40.53 dB at 9.50 GHz. Therefore, the CoNPs–G nanocomposite presents a great promising application in the electromagnetic wave absorption field.

Received 7th November 2017
Accepted 8th December 2017

DOI: 10.1039/c7ra12190c

rsc.li/rsc-advances

1. Introduction

With the development of electronic devices, electromagnetic (EM) wave interference and radiation problems are increasing, such as the harm to human bodies and information safety. The fabrication of high-efficiency EM wave absorption materials with a low density, wide effective frequency range and strong absorption properties[1–7] has attracted more and more attention in civil and military fields. There are some kinds of materials applied in EM wave absorption, for instance, ferromagnetic metals and carbon materials.

Because of the large saturation magnetization (M_s) and their Snoek limit at a high-frequency level, ferromagnetic metals and their alloys especially cobalt (Co) exhibit strong absorption intensity, whereas the frequency ranges are usually narrow.[8–15] According to the literatures, nano/microstructure Co materials, such as hollow porous cobalt spheres,[9] hierarchical sword-like cobalt particles[10] and cobalt nanoplatelets[13] with large anisotropy field have been synthesized and applied for EM wave absorption. However, the above-mentioned materials have various disadvantages when used alone. For instance, as the coating layers, the high density of metals hinders their practical applications. Moreover, they are easily oxidized and agglomerated when exposed in the air, which lead to the decrease of EM wave absorption capacity and greatly limit their application. In this direction, more advanced EM materials should be designed to provide high absorption capacity, wide absorption frequency range, light weight, good thermal stability and antioxidative capability.[16–18]

Carbon materials, such as graphite, mesoporous carbon, carbon nanotube and graphene, have attracted more attention on the EM wave absorber since World War II. They can produce eddy current under the action of electromagnetic waves and convert the electromagnetic energy into heat energy. Importantly, they can partly meet the advanced EM materials demand. Among these carbon materials, we pay more attention to graphene (G) due to its better microwave absorption properties than that of graphite and carbon nanotube.[19] G, a two-dimensional nanostructure carbon material, with large specific surface area, high conductivity, flexible, corrosion resistant and low density,[20–22] may be applied as a lightweight EM wave absorber. However, it usually exhibits low absorption property because its conductive and electromagnetic parameters are too high to meet the requirement of impedance match.[19,23,24] Adding magnetic loss nanoparticles (Co_3O_4, Fe_3O_4, Co, Ni, $NiFe_2O_4$, $CoFe_2O_4$, *etc.*) into G should be an effective method to deal with it, which can alter the values of dielectric permittivity and magnetic permeability.[25–44] Briefly, the aforementioned composites improve the absorption of electromagnetic energy due to combine the magnetic properties of ferromagnetic nanomaterials with the excellent electrical

School of Chemical Engineering, Sichuan University, Chengdu, Sichuan 610065, China. E-mail: xiekenan63@163.com

conductivity of graphene. Nevertheless, these composites are usually synthesized *via* solvothermal, hydrothermal or calcination method, which need more energy. Furthermore, the products provide EM wave absorption with single absorption peak in a certain coating thickness; on the side, only several materials[45,46] can meet the following points: the value of minimal reflection loss (RL) reached −40 dB and the effective absorption bandwidth (RL ≤ −10 dB) was ∼4 GHz simultaneously.

In this study, we exhibited a liquid phase reduction method to prepare the Co nanoparticles–graphene (CoNPs–G) nanocomposite. The CoNPs–G nanocomposite with excellent EM wave absorption properties was obtained by controlling the concentration and proportion of the reactants. In addition, the method was more simply and less energy consumption than that of solvothermal, hydrothermal and calcination methods. The microwave absorption data of the CoNPs–G nanocomposite showed that the synthetic nanocomposites held high-performance EM wave absorption with multiband, wide effective absorption bandwidth, and the possible reason was the magnetic loss of cobalt and the resistance loss of graphene.[45] To the best of our knowledge, the EM wave absorption materials of metals–graphene or metal oxide–graphene composites, which have three adsorption peaks among range of 2–18 GHz with a certain coating thickness, the effective absorption bandwidth (RL ≤ −10 dB) is more than 8 GHz, and the value of minimal reflection loss (RL) reach −40 dB, have rarely been reported. Moreover, this route will be likely to extend to the preparation of other metal–graphene EM wave absorption materials.

2. Experimental

2.1. Materials

Graphite (C, 400 mesh), potassium permanganate ($KMnO_4$), sodium nitrate ($NaNO_3$), sulfuric acid (98%, H_2SO_4), hydrogen peroxide (H_2O_2), hydrochloric acid (37.5%, HCl), cobalt chloride hexahydrate ($CoCl_2 \cdot 6H_2O$), hydrazine hydrate ($N_2H_4 \cdot H_2O$, 80 vol%), sodium hydroxide (NaOH), ethanol (99.7%, CH_3-CH_2OH) were purchased from Kelong Reagent Co., Ltd. (Chengdu, China). All chemicals were of analytical reagent grade and used as received without further purification. All aqueous solutions were prepared with de-ionized water (D.I. water).

2.2. Synthesis of samples

Graphene oxide (GO) was prepared from powdered flake graphite (400 mesh) by a modified Hummers' method as described previously. In a typical synthesis procedure, a certain amount of GO was dispersed in 10 mL D.I. water, with ultrasonication for 0.5 h. And then 4 g NaOH was added into the solution with vigorous stirring. When the solution cooled to room temperature, 10 mL a certain concentration of $CoCl_2$ solution was dropped into it. After that, 1 mL $N_2H_4 \cdot H_2O$ was added into the above solution and the reaction system was kept stirring for 1 h. After reaction, the dark precipitate was separated and washed with D.I. water and ethanol at least three times, respectively, and then dried through vacuum freeze-drying for 24 h.

2.3. Characterization

Field emission scanning electron microscope (SEM, JSM-7500F, Japan) equipped with energy dispersive X-ray spectroscopy (EDS) was applied to morphology and elemental analysis of the samples, and transmission electron microscopy (TEM, G2F20S, FEI-Tecnai, USA) was used for transmission electron microscopy analysis. The crystal structure of the as-synthesized samples was identified by X-ray diffractometer (X'Pert Pro MPD, Philips, The Netherlands), using Cu Kα ($\lambda = 0.154249$ nm) radiation. The magnetic properties of coercive force and magnetization were analyzed by a vibrating sample magnetometer (VSM, Lakeshore, model 7410 series) at 298 K. X-ray photoelectron spectroscopy (XPS, AXIS Ultra DLD, Kratos Analytical) was employed to perform surface chemical analysis and qualitative analysis of elements by using a monochromated Al Kα excitation radiation (1486.6 eV).

2.4. Electromagnetic wave absorption measurements

To investigate the EM wave absorption properties of the obtained absorbers, paraffin was selected as the matrix material. A sample containing 55 wt% of obtained samples was pressed into a ring with an outer diameter of 7 mm, thickness of 2.5–3.5 mm and an inner diameter of 3 mm for EM measurement. The complex permittivity ($\varepsilon_r = \varepsilon' - j\varepsilon''$) and relative complex permeability ($\mu_r = \mu' - j\mu''$) were determined using the T/R coaxial line method in the range of 2–18 GHz using a network analyzer (Agilent Technologies N5244A). The reflection loss (RL) curves calculated from the relative permeability and permittivity at the given frequency and absorber thickness were employed to evaluate the electromagnetic wave absorption properties.[28] The RL was calculated according to following equations:

$$Z_{in} = Z_0 \left(\frac{\mu_r}{\varepsilon_r}\right)^{\frac{1}{2}} \tan h\left[j\left(\frac{2\pi fd}{c}\right)(\mu_r\varepsilon_r)^{\frac{1}{2}}\right] \quad (1)$$

$$RL(dB) = 20\log\left|\frac{Z_{in} - Z_0}{Z_0 + Z_{in}}\right| \quad (2)$$

where f is the frequency of the electromagnetic wave, d is the thickness of absorber, c is the velocity of light, μ_r and ε_r are the relative complex permeability and permittivity, respectively, Z_0 is the impedance of free space, and Z_{in} is the input impedance of the absorber.

3. Results & discussion

CoNPs–G nanocomposite is synthesized by a facile method with the liquid reduction reaction. The synthetic process is illustrated in Fig. 1. Through the modified Hummer's method, the as-prepared GO has some functional groups such as –OH and –COOH, and these functional groups can provide it with a negative charge. When $CoCl_2 \cdot 6H_2O$ solution is added to the GO solution, Co^{2+} ions are absorbed by GO sheets *via*

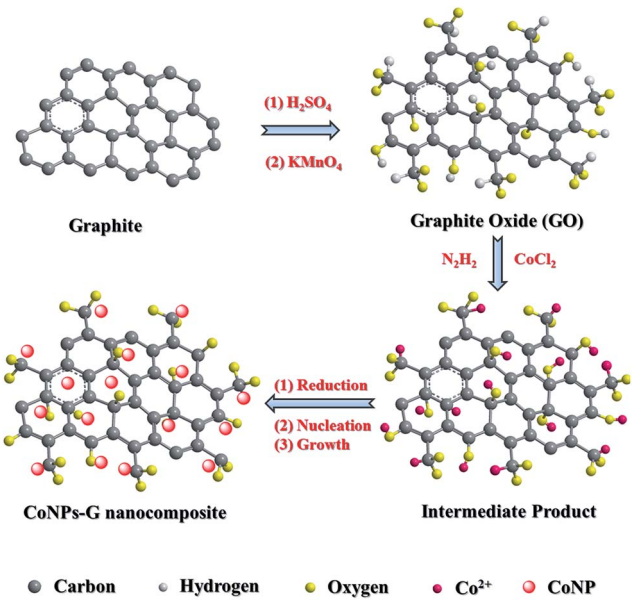

Fig. 1 Schematic illustration for preparation CoNPs–G nanocomposite.

electrostatic interaction. After the addition of $N_2H_4 \cdot H_2O$, the Co^{2+} ions of the surface of GO are reduced into Co nanoparticles first, and it also immediately drive the reduction of GO. At last the reduction of GO and the deposition of Co nanoparticles on graphene sheets take place almost simultaneously.

The phases of the as-prepared GO, G and CoNPs–G nanocomposite are investigated by XRD (Fig. 2). The diffraction peak of GO is observed at $2\theta = 9.8°$ in Fig. 2(a), indicating the distance between atomic layers of graphite is expanded to 0.80 nm. The complete oxidation of graphite into the GO makes it possible for Co to be assembled on GO sheets.[47] As shown in Fig. 2(b), the broad peak of G is $2\theta \approx 25°$, suggesting GO can be deoxygenated by hydrazine hydrate.[20] The diffraction peaks of the CoNPs–G nanocomposite are exhibited in Fig. 2(c), the peak can be assigned to the (101) plane of Co (JCPDS card no. 05-0727), and no other apparent diffraction peaks due to the impurities can be identified, implying that the high purity CoNPs–G can be obtained by this method.

The chemical component of CoNPs–G nanocomposite is further investigated by Raman. Fig. 3 exhibits the Raman spectra of GO (black line) and CoNPs–G (red line) nanocomposite. The G band is assigned to the in plane vibration of sp^2 carbon atoms, and the D band is related to the vibration of sp^3 carbon atoms. The typical G band (1593.06 cm^{-1}) and D band (1340.01 cm^{-1}) of GO are showed in picture. However, compared with GO, the G band and D band for CoNPs–G are 1596.42 cm^{-1} and 1335.54 cm^{-1}, which both have a small spectral shift. It indicates that there may be chemical interplays between the groups of G and the reactive sites of Co. As we know, the ratio of intensities of the two band ($I_D : I_G$) can be used indicate the ordered and disordered crystal structure of carbon. The $I_D : I_G$ will increase when the GO is reduced. The $I_D : I_G$ is 1.07 for GO and 1.41 for CoNPs–G. The change explains the fact that GO has been reduced to G in this experiment.

Fig. 4(a–c) show the representative SEM and TEM images of the CoNPs–G nanocomposite. From the Fig. 4(a), it can be seen that Co nanoparticles are assembled on the surface of G. In Fig. 4(b and c), the results of element mapping distribution of CoNPs–G are presented. To eliminate the probable influence from the conductive resin, the sample before testing is dropped on the Si substrate. It can be deduced that Co and C elements are uniformly distributed on the film. The presence of C element is due to the graphene. Morphology information on the CoNPs–G nanocomposite is given in Fig. 4(d–f). In the corresponding low magnification TEM images are shown in Fig. 4(d and e), G sheets are decorated randomly by Co nanoparticles. Fig. 4(e and f) show a high-resolution TEM (HRTEM) image of Co nanoparticles (marked by red circles) with a diameter approximately 5 to 10 nm. The inset of Fig. 4(f) exhibits a selected area electron diffraction (SAED) pattern, where the labeled diffraction rings can be indexed to the (101) plane of Co and the (002) plane of G,[45] respectively. In terms of the SEM, TEM and XRD analyses, CoNPs–G nanocomposite can be fabricated by our present method.

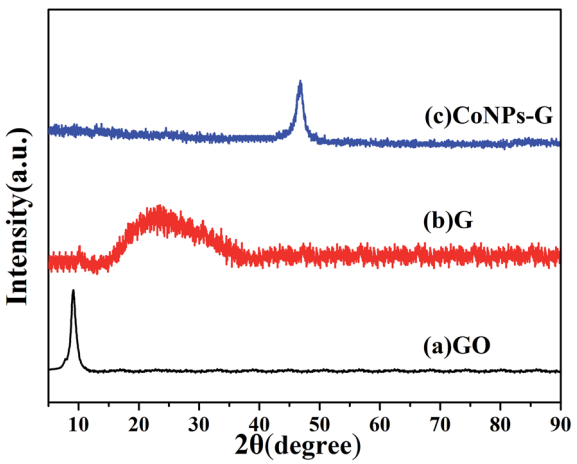

Fig. 2 XRD patterns of (a) GO, (b) G and (c) CoNPs–G nanocomposite.

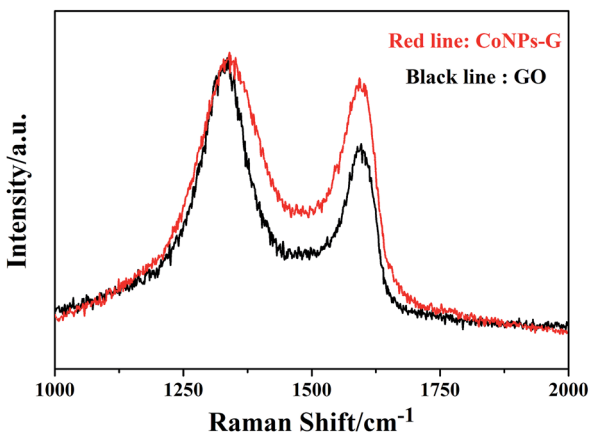

Fig. 3 Raman spectra of the pristine GO platelets and the synthesized CoNPs–G nanocomposite.

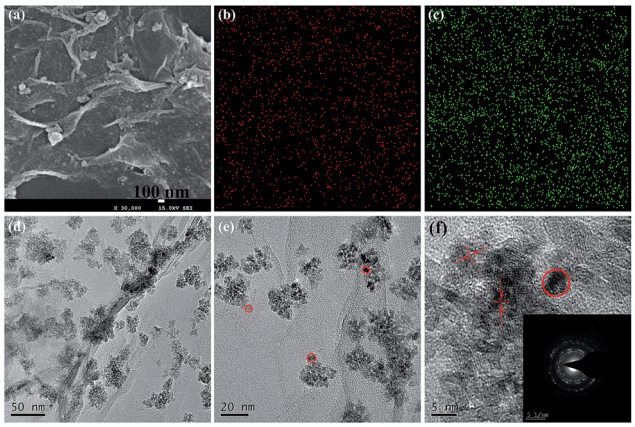

Fig. 4 SEM image (a), element distribution images of Co (b) and C (c), TEM images (d, e) and HRTEM (f) image of the CoNPs–G nanocomposite, the insets (f) show the selected area electron diffraction (SAED) patterns of the CoNPs–G nanocomposite.

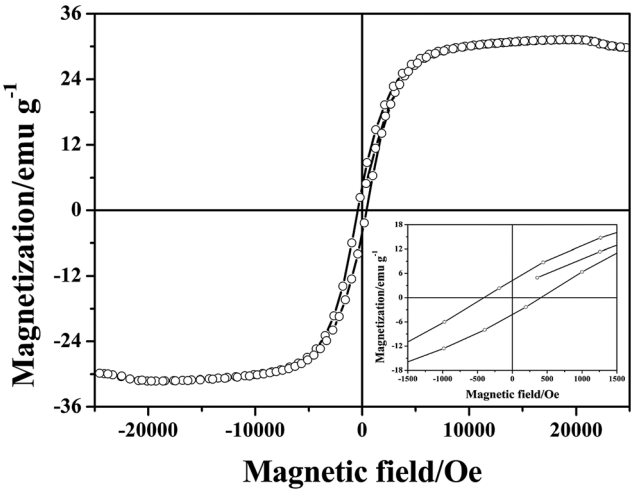

Fig. 6 The magnetic hysteresis loops of CoNPs–G nanocomposite.

The surface composition of the composite is characterized by X-ray photoelectron spectroscopy (XPS). The survey spectrum (Fig. 5(a)) shows that CoNPs–G nanocomposite consists of Co, O and C elements. C 1s XPS spectrum (Fig. 5(b)) can be deconvoluted into three peaks located at 284.5 eV, 285.6 eV and 286.7 eV, which are attributed to carbon atoms in different functional groups: C–C, C–O and C=O respectively,[48,49] indicating that GO is reduced to G, but the surface has a small number of unreducible carboxyl groups (–COOH) or hydroxyl groups (–OH). Fig. 5(c) shows the O 1s XPS spectrum of CoNPs–G nanocomposite. Two main peaks at the positions of 531.0 eV and 532.5 eV can be assigned to oxygen atoms in the surface carboxyl groups: C–O and O–C=O respectively.[50–53] In Fig. 5(d), the Co 2p peak is composed of two peaks centered at 780.2 eV and 781.4 eV. The peak at 780.2 eV should be attributed to Co $2p_{3/2}$, while the weak one at 781.4 eV corresponds to Co $2p_{1/2}$. Compared with Co $2p_{3/2}$ (778.10 eV) and Co $2p_{1/2}$ (793.3 eV), the peaks have moved to high valence, suggesting that there is a chemical bonding between Co and G rather than simple physical adsorption.

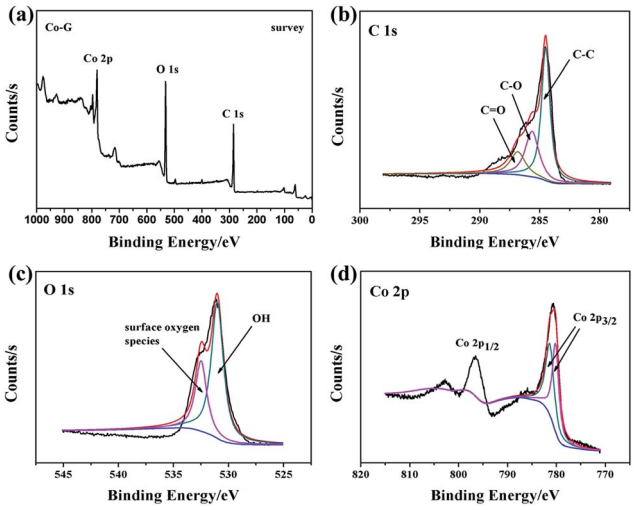

Fig. 5 XPS spectra of CoNPs–G nanocomposite: (a) survey scan; (b) C 1s region; (c) O 1s region; (d) Co 2p region.

The magnetic hysteresis loop at room temperature for the CoNPs–G nanocomposite microspheres is displayed in Fig. 6. The measured saturation magnetization (M_s) and coercivity (H_C), are 31.3 emu g^{-1} and 408.9 Oe, respectively. The smaller M_s value of CoNPs–G nanocomposite compared to bulk Co (168 emu g^{-1}, 298.15 K)[54] is mainly ascribed to the existence of graphene. On the other hand, CoNPs–G nanocomposite also shows greater coercivity (408.9 Oe) than bulk cobalt (10 Oe, 298.15 K). According to the following equation:

$$H_{c,n} = \frac{\mu}{R^3}(6K_n - 4L_n) \quad (3)$$

where μ is the magnetic dipole moment; R is the magnetic particle radius; K, L is the interaction constant between magnetic particles, and n is the number of each particle in the sphere chain model. It shows that coercivity is inversely proportional to the cube of particle radius, namely, the smaller the particle size, the greater the coercivity. The Fig. 4(e and f) shows the image of Co nanoparticles (marked by red circles) with a diameter approximately 5 to 10 nm, hence the coercivity of Co–G is greater than that of bulk Co.

The electromagnetic parameters are listed in Fig. 7. EM wave absorption properties of CoNPs–G nanocomposite are highly associated with its permittivity and permeability, where the real parts of permittivity (ε') represent the storage capability of electric energy, the imaginary parts (ε'') stand for the loss capability of electric energy, the real parts of permeability (μ') represent the degree of polarization and the imaginary parts (μ'') indicate the energy loss caused by the rearrangement of the magnetic dipole moment. In Fig. 7(a and b), the values of ε' and ε'' decrease from 16.5 to 13.2 and 2.25 to 1.05, respectively, as the frequency increases from 2 to 18 GHz range. The real parts of permittivity (ε') and the imaginary parts (ε'') both exhibit more than one resonance peaks around 6–18 GHz, which may be attributed to the interfacial polarization resonance due to the

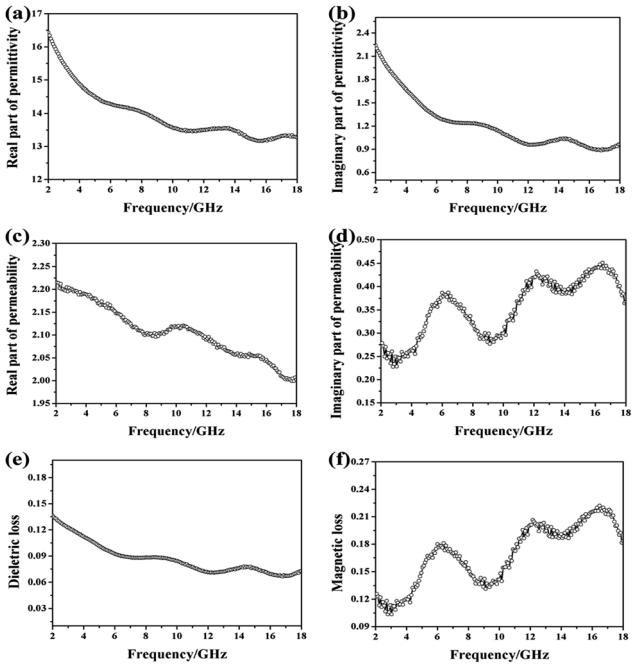

Fig. 7 The electromagnetic response of CoNPs–G nanocomposite in microwave range of 2–18 GHz: (a) real part of permittivity; (b) imaginary part of permittivity; (c) real part of permeability; (d) imaginary part of permeability; (e) dielectric loss; (f) magnetic loss.

electronegativity difference between cobalt and graphene. As shown in Fig. 7(c and d), the real parts of permeability (μ') declines from 2.11 to 1.99 with the increase frequency from 2–18 GHz, on the contrary, the imaginary parts (μ'') display wavelike rises from 0.28 to 0.36 and exhibit strong magnetic resonance peaks at 6.19, 12.16 and 16.49 GHz. The dielectric and magnetic dissipation factors, tan $\delta\varepsilon = \varepsilon''/\varepsilon'$ and tan $\delta_M = \mu''/\mu'$, respectively, provide a measure of the power lost in the EM wave absorption material *versus* the amount of power stored.[55,56] From the Fig. 7(e and f), it can be described that the dielectric loss fluctuates (from 0.14 to 0.07) slowly with the increase frequency. Moreover, the magnetic loss displays wavelike rises from 0.12 to 0.18 in 2–18 GHz frequency range, which is similar to the imaginary parts (μ''). It is interesting to note that the position of dielectric loss wave trough corresponds to that of the he magnetic loss peak. The results show that that the values of the complex relative permittivity (ε' and ε'') and permeability (μ' and μ'') were better-matched, indicating a resonance behavior, which should be conducive to the EM wave absorption performance. Besides, the dielectric loss values (tan $\delta\varepsilon = \varepsilon''/\varepsilon'$) are smaller than the magnetic loss values ($\delta_M = \mu''/\mu'$) with the increase frequency, indicating that the EM wave absorption property of CoNPs–G nanocomposite may mainly originate from its magnetic loss.

The magnetic loss type of the material can be obtained by analyzing the variation law of the function $(u''(u')^{-2} f^{-1})$. The function can be calculated according to the following equation:

$$u''(u')^{-2} f^{-1} = 2/3\pi\mu_0 d^2\sigma \quad (4)$$

where μ_0 is the vacuum permeability, σ is the electric conductivity of the composite, d is the thickness. According to the eqn (4), if the magnetic loss only stems from eddy current loss, the value of $(u''(u')^{-2} f^{-1})$ should be constant with a change in the frequency. If not, the magnetic loss is a consequence of natural resonance and exchange resonance. In Fig. 8, the value of $(u''(u')^{-2} f^{-1})$ varies with the frequency, which means the magnetic

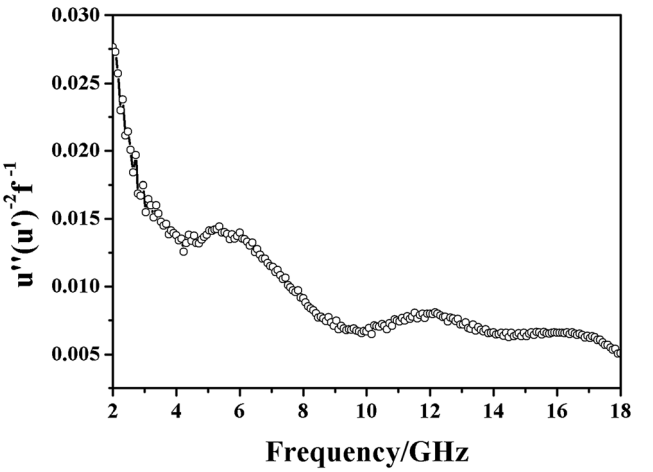

Fig. 8 Frequency dependence of $(u''(u')^{-2} f^{-1})$ in 2–18 GHz frequency range.

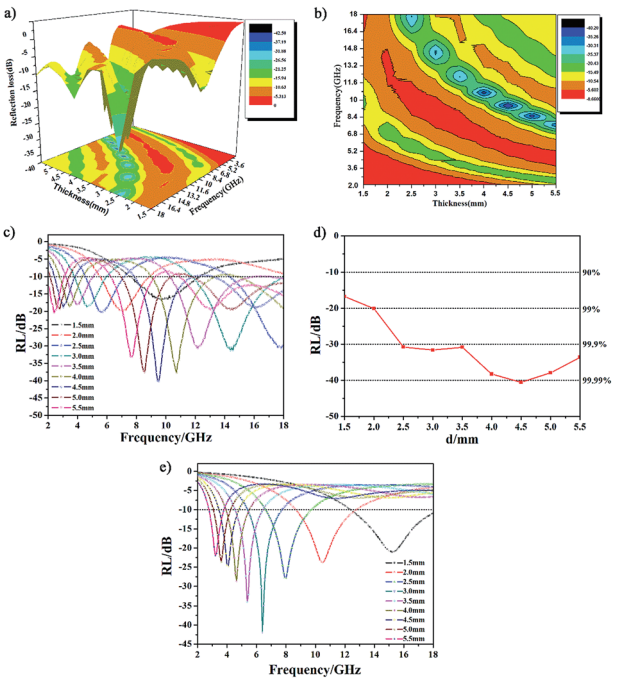

Fig. 9 The microwave absorption properties of CoNPs–G nanocomposite in 2–18 GHz frequency range: (a) three-dimensional representation, and (b) two dimensional colorful map representation of RL for CoNPs–G nanocomposite with different thickness, (c) RL of CoNPs–G nanocomposite *vs.* frequency at different thicknesses, (d) RL_{max} of CoNPs–G nanocomposite with different thickness, (e) RL of CoNPs (55 wt% in the paraffin matrix) *vs.* frequency at different thicknesses.

Table 1 Comparison of microwave absorption properties between as-prepared CoNPs–G nanocomposite and other representative metal–graphene composites

Sample	RL_{max} (dB)	Bandwidth (RL < −10 dB) (GHz)	Frequency range (RL < −10 dB) (GHz)	Ref.
CoNPs–G	−40.53	10.22	7.84–11.87, 2.4–3.84, 13.25–18	This work
Co particle	−60.13	5.42	11.87–17.85	10
RGO/NiO	−55.5	6.7	10.2–16.9	25
RGO–Co_3O_4	−43.7	4.6	3.6–5.4, 12.3–15.1	26
Graphene	−6.5	0	0	60
NiO–G	−59.6	4.24	12.48–16.72	61
Fe–G	−45	2.5	6.0–8.5	62
Co particle	−48.03	6.67	—	63
Nanoporous carbon	42.4	1.76	8.08–9.84	64
CuO/carbon	57.5	4.7	13–17.7	65
MWCNTs	26.9	4.24	12.48–16.72	66

loss of the CoNPs–G nanocomposite is attributed to the synergy effects of natural resonance and exchange resonance, which are beneficial to widen the bandwidth of microwave absorption.[10] The first resonance peak at 5.36 GHz is due to natural resonance, which would occur in magnetic particles when the frequency of incident microwave can be line with the intrinsic frequency of the magnetization spinning oscillation. The two resonance peaks at 11.52 and 16.48 GHz is ascribed to exchange resonance. It can be discussed with the exchange resonance mode developed by Aharoni.[57–59] The frequency exchange resonance of magnetic materials is determined by their particle size, morphology and the composition.

The microwave absorption properties of CoNPs–G nanocomposite are illustrated in Fig. 9. A 3D image map and a contour map of RL for CoNPs–G nanocomposite are shown in Fig. 9(a) and (b). It can be observed that the material displayed superior microwave absorption performance in both the value of RL and absorption width. There existed three excellent microwave absorption "green gorge" and "yellow islands" in the two figures, respectively, which covered almost half of the map area. Fig. 9(c) shows the frequency-dependent RL curves of the CoNPs–G nanocomposite with addition amount of 55 wt% in the paraffin matrix at different thicknesses (d = 1.5–5.5 mm). Compared with Fig. 9(e), the frequency-dependent RL curves of the CoNPs, it can be found that most RL curves of the CoNPs–G nanocomposite have at least two peaks except for the coating thickness of CoNPs–G nanocomposite at 1.5 mm and 2 mm. The minimal RL value is up to −40.53 dB at 9.5 GHz at d = 4.5 mm, which the effective absorption bandwidth (RL ≤ −10 dB) is 4.03 GHz, and the other two peaks of this RL curve appear at 3.04 GHz and 16.13 GHz, the minimal RL value is −18.82 dB and −18.95 dB, respectively. Moreover, the broad effective bandwidth reached the maximum of 10.22 GHz, which covered the S, X, and Ku band at a single thickness, and to our best knowledge, no previous literature reported it. By adjusting the thickness, the effective absorption bandwidth could cover almost all the S, C, X, and Ku band. It can be seen from the Fig. 9(d) that the coating thickness of CoNPs–G nanocomposite has great influence on its minimal RL. First, the value of RL decrease with the increase coating thickness, then it increases when the coating thickness is beyond 4.5 mm. Furthermore, compared with other recently reported materials, the CoNPs–G nanocomposite has more wider operation absorption bandwidth, and effective absorption range has covered the whole frequency from 2 to 18 GHz. Notably, the introduction of graphene in Co nanoparticles can improve its EM wave absorption performance, including high absorption efficiency, wide operation absorption bandwidth, and multiband absorption function, as shown in Table 1.

4. Conclusions

In summary, CoNPs–G nanocomposite was synthesized *via* a facile liquid reduction method. Multiple dielectric, magnetic resonance peaks were exhibited in the microwave range of 2–18 GHz. The natural resonance and exchange resonance of the material were beneficial to widen the bandwidth of microwave absorption. In particular, three effective RL peaks across low, middle and high frequencies (2.4–3.84, 7.84–11.87 and 13.25–18 GHz), had been observed in the curve with the coating thickness of 4.5 mm, the minimal RL reached −40.53 dB at 9.50 GHz, and the widest effective absorption bandwidth was 10.22 GHz. The effective absorption bandwidth could cover almost all the S, C, X and Ku band with the thickness in the range of 1.5–5.5 mm, which indicated that the CoNPs–G nanocomposite has potential application for EM wave absorption.

Conflicts of interest

There are no conflicts to declare.

References

1 M. Okoniewski and M. A. Stuchly, *IEEE Trans. Microwave Theory Tech.*, 1996, **44**, 1855–1864.
2 A. Hirata, S. I. Matsuyama and T. Shiozawa, *IEEE Trans. Electromagn. Compat.*, 2000, **42**, 386–393.
3 J. Joo and A. J. Epstein, *Appl. Phys. Lett.*, 1994, **65**, 2278–2280.
4 G. Sun, B. Dong, M. Cao, B. Wei and C. Hu, *Chem. Mater.*, 2011, **23**, 115–118.
5 G. Wang, Z. Gao, S. Tang, C. Chen, F. Duan, S. Zhao, S. Lin, Y. Feng, L. Zhou and Y. Qin, *ACS Nano*, 2012, **6**, 11009–11017.

6 X. F. Zhang, X. L. Dong, H. Huang and Y. Y. Liu, *Appl. Phys. Lett.*, 2006, **89**, 053113–053115.
7 J. Jiang, D. Li, D. Geng, J. An, J. He, W. Liu and Z. Zhang, *Nanoscale*, 2014, **6**, 3967–3971.
8 V. B. Bregar, *IEEE Trans. Magn.*, 2005, **36**, 1679–1684.
9 C. He, S. Qiu, X. Wang, J. Liu, L. Luan, W. Liu, M. Itoh and K. Machida, *J. Mater. Chem.*, 2012, **22**, 22160–22166.
10 S. Wen, X. Zhao, Y. Liu, J. Cheng and H. Li, *RSC Adv.*, 2014, **4**, 40456–40463.
11 S. S. Kim, S. T. Kim, J. M. Ahn and K. H. Kim, *J. Magn. Magn. Mater.*, 2004, **271**, 39–45.
12 J. R. Liu, M. Itoh and K. Machida, *Appl. Phys. Lett.*, 2006, **88**, 062503–062506.
13 J. Li, J. Huang, Y. Qin and F. Ma, *Mater. Sci. Eng., B*, 2007, **138**, 199–204.
14 X. Tang, Q. Tian, B. Zhao and K. Hu, *Mater. Sci. Eng., A*, 2007, **445–446**, 135–140.
15 Y. Yang, C. Xu, Y. Xia, T. Wang and F. Li, *J. Alloys Compd.*, 2010, **493**, 549–552.
16 Z. Guo, S. E. Lee, H. Kim, S. Park, H. T. Hahn, A. B. Karki and D. P. Young, *Acta Mater.*, 2009, **57**, 267–277.
17 F. Wang, J. Liu, J. Kong, Z. Zhang, X. Wang, M. Itoh and K. Machida, *J. Mater. Chem.*, 2011, **21**, 4314–4320.
18 S. C. Chiu, H. C. Yu and Y. Y. Li, *J. Phys. Chem. C*, 2010, **114**, 1947–1952.
19 C. Wang, X. Han, P. Xu, X. Zhang, Y. Du, S. Hu, J. Wang and X. Wang, *Appl. Phys. Lett.*, 2011, **98**, 217.
20 Y. Yang, M. C. Gupta, K. L. Dudley and R. W. Lawrence, *Nano Lett.*, 2005, **5**, 2131–2134.
21 Y. Huang, Z. Xu, J. Shen, T. Tang and R. Huang, *Appl. Phys. Lett.*, 2007, **90**, 971.
22 K. Chen, C. Xiang, L. Li, H. Qian, Q. Xiao and F. Xu, *J. Mater. Chem.*, 2012, **22**, 6449–6455.
23 K. S. Novoselov, A. K. Geim, S. V. Morozov, D. Jiang, Y. Zhang, S. V. Dubonos, I. V. Grigorieva and A. A. Firsov, *Science*, 2004, **306**, 666–669.
24 L. Kong, X. Yin, Y. Zhang, X. Yuan, Q. Li, F. Ye, L. Cheng and L. Zhang, *J. Phys. Chem. C*, 2017, **117**, 19701–19711.
25 H. Zhang, X. Tian, C. Wang, H. Luo, J. Hu, Y. Shen and A. Xie, *Appl. Surf. Sci.*, 2014, **314**, 228–232.
26 H. Lv, Y. Guo, Z. Yang, Y. Cheng, L. P. Wang, B. Zhang, Y. Zhao, Z. J. Xu and G. Ji, *J. Mater. Chem. C*, 2016, **5**, 491–512.
27 H. Lv, G. Ji, X. H. Liang, H. Zhang and Y. Du, *J. Mater. Chem. C*, 2015, **3**, 5056–5064.
28 Z. Zhu, X. Sun, H. Xue, H. Guo, X. Fan, X. Pan and J. He, *J. Mater. Chem. C*, 2014, **2**, 6582–6591.
29 P. Liu, Y. Huang, L. Wang, M. Zong and W. Zhang, *Mater. Lett.*, 2013, **107**, 166–169.
30 A. Gupta, A. P. Singh, S. Varshney, N. Agrawal, P. Sambyal, Y. Pandey, B. P. Singh, V. N. Singh, B. K. Gupta and S. K. Dhawan, *RSC Adv.*, 2014, **4**, 62413–62422.
31 Y. Chen, Z. Lei, H. Wu, C. Zhu, P. Gao, Q. Ouyang, L. H. Qi and W. Qin, *Mater. Res. Bull.*, 2013, **48**, 3362–3366.
32 G. Pan, J. Zhu, S. Ma, G. Sun and X. Yang, *ACS Appl. Mater. Interfaces*, 2013, **5**, 12716–12724.
33 Y. Cao, Q. Su, R. Che, G. Du and B. Xu, *Synth. Met.*, 2012, **162**, 968–973.
34 W. L. Song, X. T. Guan, L. Z. Fan, W. Q. Cao, Q. L. Zhao, C. Y. Wang and M. S. Cao, *Mater. Res. Bull.*, 2015, **72**, 316–323.
35 B. Qu, C. Zhu, C. Li, X. Zhang and Y. Chen, *ACS Appl. Mater. Interfaces*, 2016, **8**, 3730–3735.
36 G. S. Wang, Y. Wu, Y. Z. Wei, X. J. Zhang, Y. Li, L. D. Li, B. Wen, P. G. Yin, L. Guo and M. S. Cao, *ChemPlusChem*, 2014, **79**, 375–381.
37 C. Hu, Z. Mou, G. Lu, N. Chen, Z. Dong, M. Hu and L. Qu, *Phys. Chem. Chem. Phys.*, 2013, **15**, 13038–13043.
38 M. Fu, Q. Jiao and Y. Zhao, *J. Mater. Chem. A*, 2013, **1**, 5577–5586.
39 M. Fu, Q. Jiao, Y. Zhao and H. Li, *J. Mater. Chem. A*, 2013, **2**, 735–744.
40 T. Wang, Z. Liu, M. Lu, B. Wen, Q. Ouyang, Y. Chen, C. Zhu, P. Gao, C. Li and M. Cao, *J. Appl. Phys.*, 2013, **113**, 666.
41 Y. Ren, C. Zhu, S. Zhang, C. Li, Y. Chen, P. Gao, P. Yang and Q. Ouyang, *Nanoscale*, 2013, **5**, 12296–12303.
42 Y. L. Ren, H. Y. Wu, M. M. Lu, Y. J. Chen, C. L. Zhu, P. Gao, M. S. Cao, C. Y. Li and Q. Y. Ouyang, *ACS Appl. Mater. Interfaces*, 2012, **4**, 6436–6442.
43 H. Zhang, C. Zhu, Y. Chen and H. Gao, *ChemPhysChem*, 2014, **15**, 2261.
44 C. Zhu, S. Zhang, Y. Sun and Y. Chen, *J. Alloys Compd.*, 2017, **711**, 552–559.
45 T. Chen, F. Deng, J. Zhu, C. Chen, G. Sun, S. Ma and X. Yang, *J. Mater. Chem.*, 2012, **22**, 15190–15197.
46 X. Wang, J. Yu, H. Dong, M. Yu, B. Zhang, W. Wang and L. Dong, *Appl. Phys. A*, 2015, **119**, 1483–1490.
47 Z. H. Liu, Z. M. Wang, X. Yang and K. Ooi, *Langmuir*, 2002, **18**, 4926–4932.
48 Z. Ji, X. Shen, Y. Song and G. Zhu, *Mater. Sci. Eng., B*, 2011, **176**, 711–715.
49 S. Stankovich, D. A. Dikin, R. D. Piner, K. A. Kohlhaas, A. Kleinhammes, Y. Jia, Y. Wu, S. B. T. Nguyen and R. S. Ruoff, *Carbon*, 2007, **45**, 1558–1565.
50 J. J. Yang, H. Cheng and R. L. Frost, *Spectrochim. Acta, Part A*, 2011, **78**, 420–428.
51 J. Stoch and J. Gablankowska-Kukucz, *Surf. Interface Anal.*, 2004, **17**, 165–167.
52 B. Varghese, C. H. Teo, Y. Zhu, M. V. Reddy, B. V. R. Chowdari, A. T. S. Wee, V. B. C. Tan, C. T. Lim and C. H. Sow, *Adv. Funct. Mater.*, 2010, **17**, 1932–1939.
53 S. C. Petitto, E. M. Marsh, G. A. Carson and M. A. Langell, *J. Mol. Catal. A: Chem.*, 2008, **281**, 49–58.
54 H. Chen, C. Xu, X. Zhou, Y. Liu and G. Zhao, *Mater. Res. Bull.*, 2012, **47**, 4353–4358.
55 Z. Fan, G. Luo, Z. Zhang, L. Zhou and F. Wei, *Mater. Sci. Eng., B*, 2006, **132**, 85–89.
56 D. L. Zhao, X. Li and Z. M. Shen, *Compos. Sci. Technol.*, 2008, **68**, 2902–2908.
57 A. Aharoni, *J. Appl. Phys.*, 1991, **69**, 7762–7764.
58 A. Aharoni, *J. Appl. Phys.*, 1997, **81**, 830–833.
59 A. Aharoni, *J. Appl. Phys.*, 1994, **76**, 6977–6979.
60 J. J. Fang, L. I. Sufang, W. K. Zha, H. Y. Cong, J. F. Chen and Z. Z. Chen, *J. Inorg. Mater.*, 2011, **26**, 467–471.

61 L. Wang, H. Xing, S. Gao, X. Ji and Z. Shen, *J. Mater. Chem. C*, 2017, **5**, 2005–2014.
62 X. Zhao, Z. Zhang, L. Wang, K. Xi, Q. Cao, D. Wang, Y. Yang and Y. Du, *Sci. Rep.*, 2013, **3**, 3421.
63 S. L. Wen, Y. Liu, X. C. Zhao, J. W. Cheng and H. Li, *Phys. Chem. Chem. Phys.*, 2014, **16**, 18333–18340.
64 X. Qiu, L. Wang, H. Zhu, Y. Guan and Q. Zhang, *Nanoscale*, 2017, **9**, 7408–7418.
65 J. Ma, X. Zhang, W. Liu and G. Ji, *J. Mater. Chem. C*, 2016, **4**, 11419–11426.
66 S. Yun, A. Kirakosyan, S. Surabhi, J. R. Jeong and J. Choi, *J. Mater. Chem. C*, 2017, **5**, 8436–8442.